Research Article

Electrical properties of barium titanate in presence of Sn²⁺ dopant

Richa Tomar[1] · Rahul Pandey[1] · N. B. Singh[1,2] · Manoj Kumar Gupta[3] · Pankaj Gupta[1,4]

Abstract

The properties of $BaTiO_3$ based ferroelectrics can be enhanced by appropriate doping. $BaTiO_3$ and Sn doped $BaTiO_3$ were synthesized using sol–gel route and characterized by X-ray diffraction technique. Microstructural evaluation was done by scanning electron microscopy. On doping with Sn, the dielectric permittivity of the material is increased 3 times to that of the pure $BaTiO_3$ and a very low dielectric loss of < 1 was observed. Tin doped $BaTiO_3$ can act as a promising material for piezoelectric applications because of high T_c (292 °C).

Keywords Doping · Dielectric properties · Relaxor behavior · Piezoelectric

1 Introduction

Lead free piezoelectric materials have attracted considerable attention of researchers during the recent years [1]. Barium titanate ($BaTiO_3$) is one such material studied extensively. This has perovskite structure with various properties and applications [2]. It has high dielectric constant also. On doping various ions in barium titanate, properties are changed [3]. On doping isovalent ions on both sites of A(Ba) and B(Ti), electrical and dielectric properties are affected considerably [3]. When Ti^{4+} is replaced by Sn^{4+}, interesting properties are seen [4, 5]. On doping Sn^{4+} in barium titanate, microstructure and electrical properties are changed considerably [6]. However, limited studies on the properties of barium titanate in presence of Sn^{2+} as dopant has been made [7]. Doping plays an important role in changing the structural, electronic and optical properties of the materials [8–12].

It is expected that if Ba^{2+} ion is replaced by ions of smaller size, the motion of the Ti^{4+} ion on the octahedral site will be reduced. The ionic radii of Ba^{2+} and Sn^{2+} are respectively 146 pm and 118 pm, so if Sn^{2+} is used as doping agent, the properties of $BaTiO_3$ (BT) will be changed.

In this paper, BT has been prepared by sol–gel technique using Sn^{2+} as dopant. Electrical conductivity and dielectric constant have been determined at different temperatures and frequencies. Results have been discussed.

2 Experimental

2.1 Materials

$Ba(CH_3COO)_2$ (Sigma-Aldrich, CAS No. 513-77-9, 99.9%), titanium alkoxide $Ti[OCH(CH_3)_2]_4$ (Sigma-Aldrich, CAS No. 13463-67-7, 99.9%), hydrated stannous chloride ($SnCl_2.2H_2O$) (Sigma-Aldrich, CAS No. 278513-25G, 99.9%), glacial acetic acid (Merck, 100%, CAS No. 64-19-7), Isopropanol (Alfa Aesar, CAS No. 67-63-0, 99+ %), Titanium tetraisopropoxide (TTIP) (Sigma-Aldrich, CAS No. 13463-67-7, 99.9%) were used as such without further purification.

2.2 Synthesis route

$BaTiO_3$ doped with Sn^{2+} was synthesized by sol–gel route. Barium acetate and hydrated stannous chloride

(20%) in molar ratio of 1:6 were dissolved in acetic acid at 65 °C in a round bottom flask and the solution was allowed to cool to room temperature. 2-Propanol was added to the solution with stirring for an hour. TTIP was also added. The mixture was cooled to 2–3 °C and deionized water was mixed. 2-Propanol/titanium tetraisopropoxide/acetic acid/water mole ratio of 1:1:6:150 was used. Finally yellow color sol was formed which was stirred for homogenization for a period of 3 h. After the completion, the gel was dried at 100 °C. Thereafter, the xerogels were calcined at different temperatures to obtain nanocrystalline Sn doped $BaTiO_3$.

2.3 Material characterization

The powder X-ray diffraction studies were performed by X 'Pert PRO using CuK_α radiation (45 kV and 40 mA) at a speed of 2°/min over the range 10–60°. The surface morphology of obtained powder was investigated by Scanning Electron Microscopy (SEM) and energy dispersive X-ray spectroscopy using a JEOLT330 microscope. Dielectric constant and electrical conductivity were measured as a function of frequency (100–1000 kHz) and temperature (RT-400 °C). The measurements were made with Agilent E4980A LCR meter on a cylindrical pellet of dimension 0.7 mm (thickness) × 4 mm (diameter) made using hydraulic press at a pressure of 5 ton. Silver paste was used for a contact.

3 Results and discussion

3.1 X-ray diffraction

Powder X-ray diffraction pattern of Sn doped $BaTiO_3$ prepared at 1200 °C is shown in Fig. 1. All the diffraction peaks of undoped $BaTiO_3$ can be indexed for tetragonal structure using JCPDS number 00-005-0626 while the doped $BaTiO_3$ has cubic structure with space group Pm-3 m. The disappearance of (002) and (210) peaks suggests phase change [13]. All the peaks in the presence of Sn^{2+} are slightly shifted showing the formation of solid solution [7]. As there is difference in the ionic radii of Ba^{2+} and Sn^{2+} (ionic radii of Ba^{2+} is 1.46 Å and Sn^{2+} is 1.18 Å), it will decrease the size of dodecahedral cavity [14] and the lattice will contract to some extent. The decrease in 2θ values shows that some of the Sn^{2+} has been oxidized to Sn^{4+} and might have replaced Ti^{4+}. The slight shift in the main intense peak is shown in inset of Fig. 1. The presence of well defined and intense peaks shows high degree of crystallinity. The absence of any extra peak discards the possibility of any secondary phase which suggests that $SnCl_2$ is completely incorporated into the $BaTiO_3$ matrix forming solid solution [7].

3.2 SEM

The SEM image of the sample heated at 1200 °C is shown in Fig. 2. The figure shows uniform distribution of the particles in the nano range (< 200 nm). The EDX pattern shows the presence of Sn (16.21%). Insertion of Sn at

Fig. 1 Powder X-ray diffraction patterns of $BaTiO_3$ and Sn-doped $BaTiO_3$ at 1200 °C
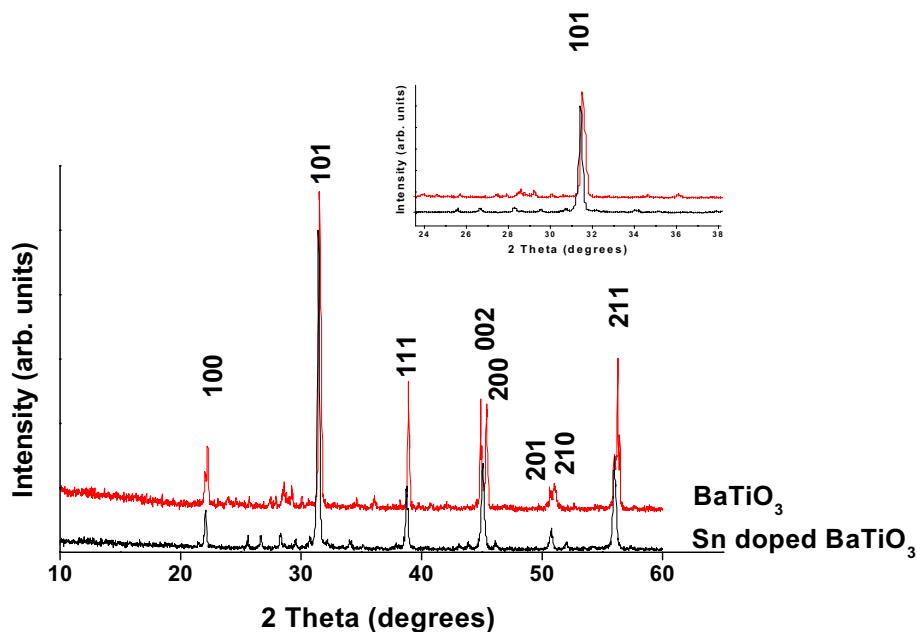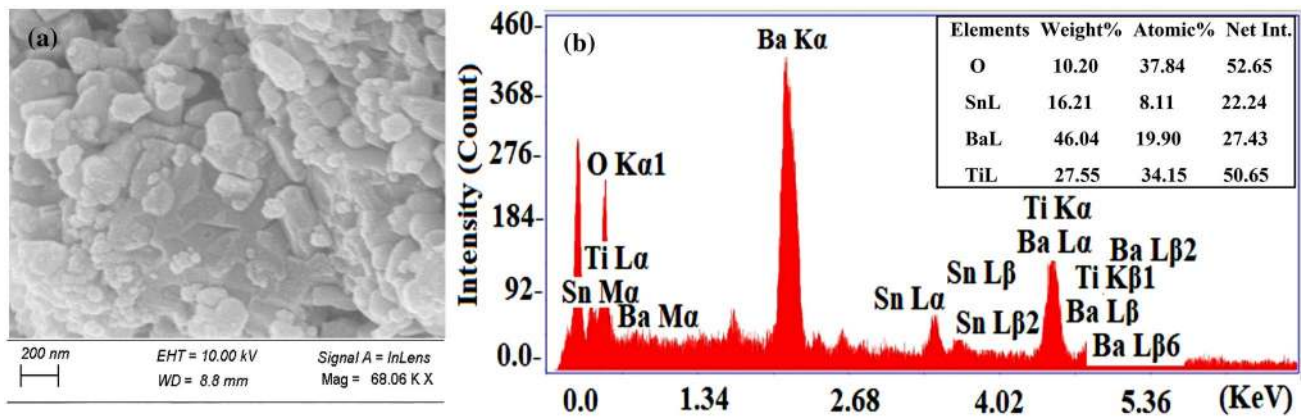
Fig. 2 **a** SEM image of Sn doped BaTiO$_3$ at 1200 °C and **b** EDX image

place of Ba and Ti leads to point defects and distortion which yields strain energy. In order to reduce surface free energy, movement of atoms from particles of smaller radii to larger radii takes place resulting in irregular grains. The formation energy of oxygen vacancies to certain extent and grain boundary diffusion coefficient is enhanced by decrease in strain energy [6]. With increased defects the mass transport process is improved leading to increased diffusion and leads to particles of variable shape and size as can be seen in Fig. 2a.

3.3 Dielectric properties

Figure 3 shows the variation of dielectric constant of undoped and Sn doped BaTiO$_3$ as a function of temperature at different frequencies. Variation of dielectric constant with temperature does not show any peak but Sn doped BaTiO$_3$ shows a sharp peak (288 as relative permittivity) at 292 °C and 500 MHz frequency. The figure shows the decrease in peak maxima with the rise in frequency.

The increase in dielectric constant in Sn doped BaTiO$_3$ with temperature is because of space charge polarization. The higher value of dielectric constant of doped BaTiO$_3$ at low frequencies may be due to the contribution of dipolar, electronic, ionic and space charge polarization, which depend on the frequencies. The increase in relative permittivity with temperature shows the increase in interfacial polarization and maximum value of relative permittivity is observed from ferro to paraelectric phase transition. Polarization is storage of charge in dielectric materials in presence of electric filed. There is very small effect of temperature on ionic and electronic polarization [15].

In such materials, changes in dielectric constant have been reported at around 60 °C and 125 °C due to orthorhombic to tetragonal and tetragonal to cubic phase transitions respectively, showing ferroelectric behavior [16, 17]. In Fig. 3 such two transitions can easily be observed with extended existence of tetragonal phase. However, tetragonal to cubic phase transition is occurring at 292 °C instead of 125 °C, making it a possible material

Fig. 3 Dielectric constant of **a** BaTiO$_3$ and **b** Sn doped BaTiO$_3$ as a function of temperature at different frequencies
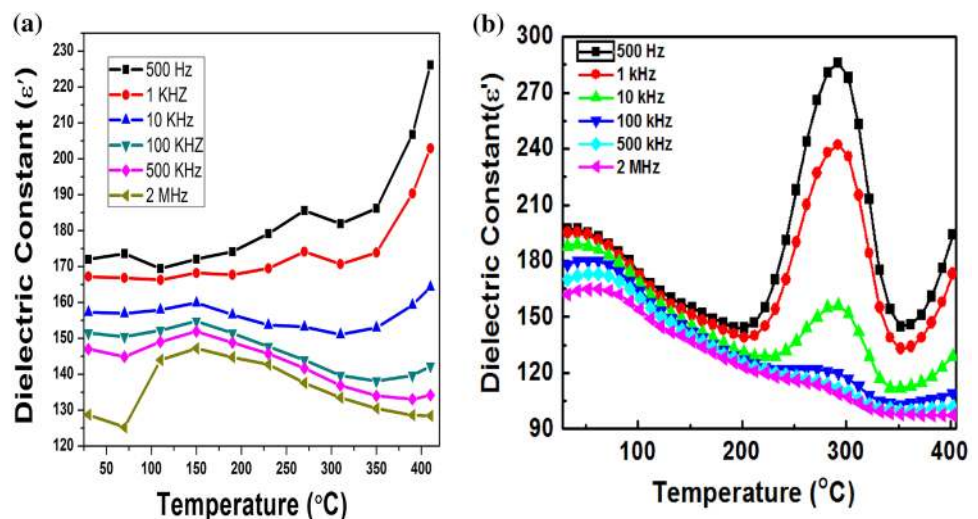
for piezoelectric devices. The first dielectric peak T_d (depolarization temperature) corresponds to the change from ferroelectric phase to antiferroelectric phase while T_c corresponds to a change from antiferroelectric phase to paraelectric phase.

It is being observed that the dielectric constant decreases with the increase in frequency and increases with increase in temperature till 150 °C in case of $BaTiO_3$ and till 280 °C in case of Sn doped $BaTiO_3$ as seen in Fig. 4. The reported Curie temperature of $BaTiO_3$ is 130 °C [18]. Important observation is that the dielectric constant of $BaTiO_3$ obtained is 100 which is lower than the dielectric constant noticed for Sn-doped $BaTiO_3$ i.e. 400 at 280 °C. The dielectric constant increased 3 times on doping with Sn. Most of the Sn^{2+} ions are likely to enter at A-site due to small ionic radii of Sn^{2+} (1.18 Å) than that of Ba^{2+} (1.46 Å). In the present case Sn^{2+} ions act as donor and create the cation vacancies in $BaTiO_3$, which increase the oxygen vacancies. The main cause of domain wall clamping are these oxygen vacancies. Dielectric permittivity increased with increase in temperature. With increase in temperature, the

oxygen vacancies could be thermally "ionized", their conduction would become dominant due to their mobility, higher vacancy concentration and higher inertia of oxygen ions. This would lead ultimately to higher dielectric permittivity value [19]. So, the high dielectric permittivity of doped samples is due to crystal imperfections formed by doping [20].

The $BaTiO_3$ ceramics are used in sonars due to their high electromechanical coupling factor and peizo electric strain constant, but due to low curie temperature of 130 °C, it is not a suitable material for piezoelectric applications [21]. Tin doped $BaTiO_3$ can act as a promising material for piezoelectric applications because of high T_c. Figure 5 presents the variation of dissipation factor with applied frequency and a very low tan δ of ~ 0.01 was detected at higher frequency side. Dielectric loss increases with the increase of the temperature. The slightly difference in dielectric loss in undoped and doped $BaTiO_3$ can be attributed to the presence of oxygen vacancies.

Curie–Weiss law and Lorentz equations were used to evaluate the exact temperature where the dielectric

Fig. 4 Dielectric constant of **a** $BaTiO_3$ and **b** Sn doped $BaTiO_3$ as a function of frequency at different temperatures
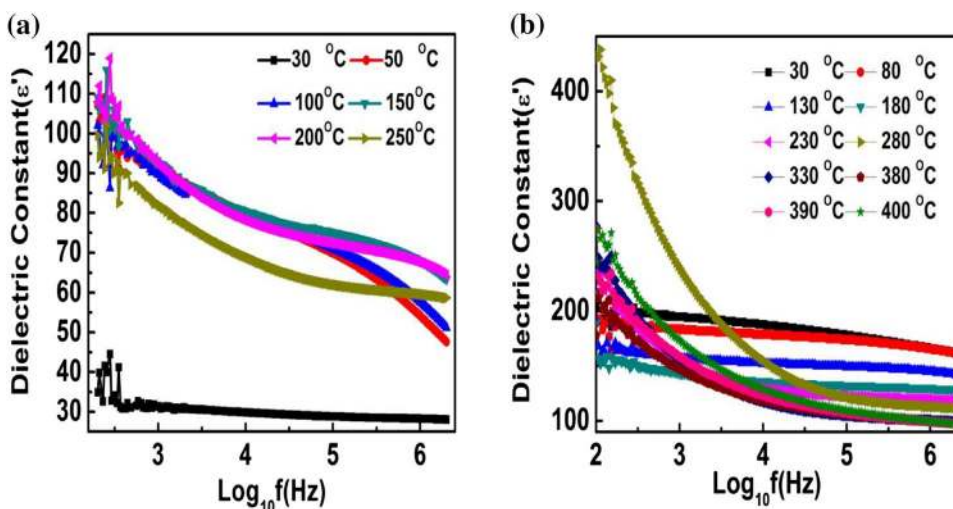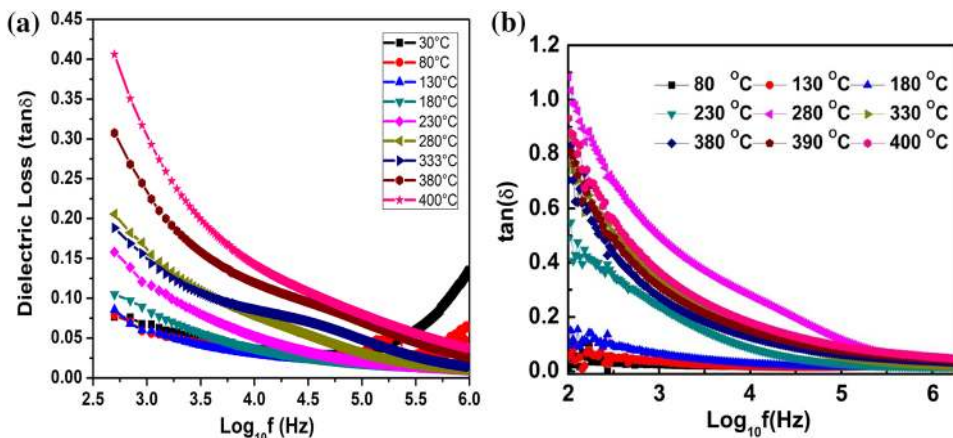
Fig. 5 Variation of dielectric loss with frequencies at different temperatures for **a** $BaTiO_3$ and **b** Sn doped $BaTiO_3$

constant was maximum (Fig. 6). For a normal ferroelectric, Curie–Weiss law equation (Eq. 1) holds good:

$$1/\varepsilon' = (T - T_{CW})/C \tag{1}$$

T_{CW} is the Curie–Weiss temperature and C is the Curie constant. From the linear fit between $1/\varepsilon'$ and T for Sn doped BaTiO$_3$, value of T_{CW} and $1/\varepsilon'_m$ at 500 Hz and 1 kHz were found to be 292C 0.00352 and 292 °C, 0.0041, respectively. In order to demonstrate the presence of relaxor type ferroelectric structure in this sample, Eq. 2 was used.

$$\log\left(1/\varepsilon - 1/\varepsilon_m\right) = \gamma\{\log\left(T - T_m\right)/C\} \tag{2}$$

where γ is the diffuseness exponent whose value range from 1 to 2. The variation of log ($1/\varepsilon - 1/\varepsilon_m$) with {log (T-T$_m$)/C} for the Sn doped BaTiO$_3$ at frequency 500 Hz and 1 kHz has been presented in Fig. 6. The γ value was calculated from the slope after fitting the curve linearly. The diffusion factor γ was found to be 1.08 and 1.50 at 500 Hz and 1 kHz, respectively. This suggested the relaxor type ferroelectric behavior in this system.

Figure 7 shows variation of a. c. conductivity with frequency at different temperatures on log scale. AC conductivity of the material was calculated using the formula

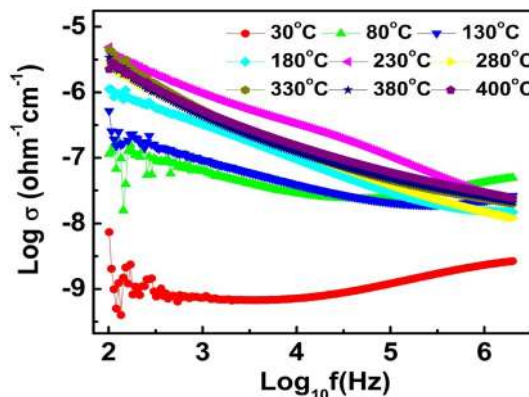$$\sigma = 2\pi f \varepsilon_o \varepsilon \tan\,\delta \tag{3}$$

Fig. 7 Graphs of Log (conductivity) versus Log (frequency) at different temperatures for Sn doped BaTiO$_3$

where, f is the applied frequency, tan δ is dielectric loss and ε_o and ε are the dielectric constants of free space and sample, respectively. It can be observed that ac conductivity of Sn doped BaTiO$_3$ increases from the low frequency region to the high frequency region and the conductivity follows the Jonscher power law relation

$$\sigma_{ac} = \sigma_{dc} + A\omega^s \tag{4}$$

where ω is the angular frequency, A is a constant and the exponent s is a frequency dependent parameter having

Fig. 6 **a** and **b** Dielectric constant data fitting with the Lorentz type quadratic equation, **c** and **d** Dielectric constant data fitting to the modified Curie–Weiss law
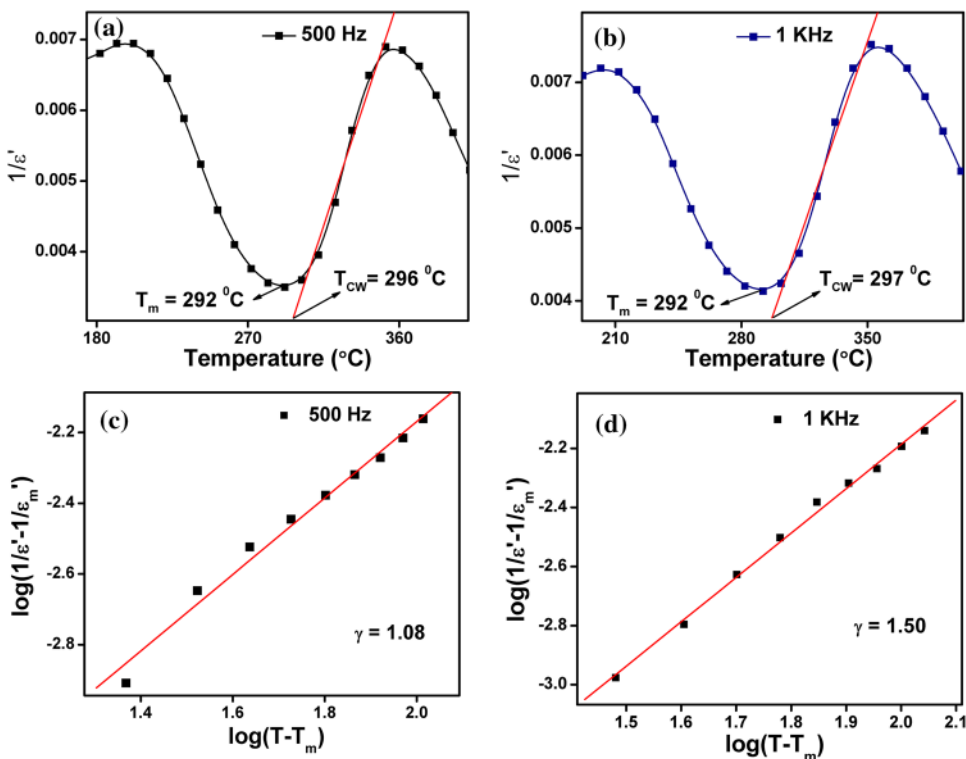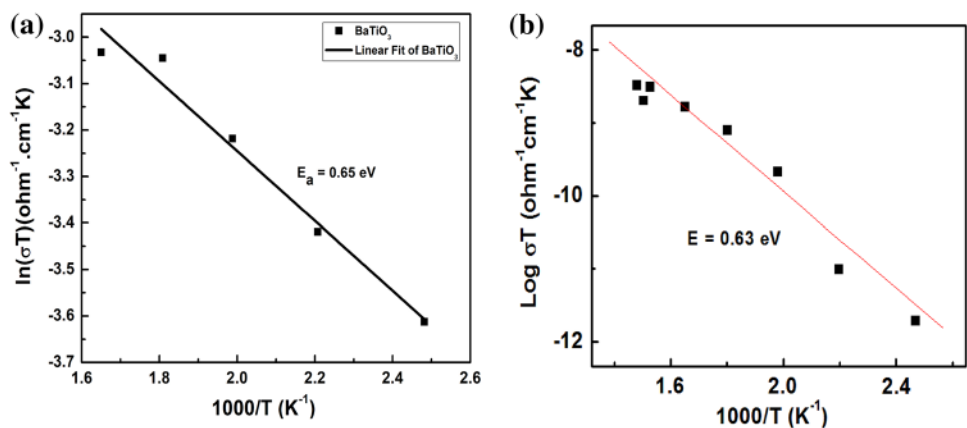
Fig. 8 Arrhenius plot between log(conductivity) versus 1/T for **a** BaTiO$_3$ and **b** Sn doped BaTiO$_3$
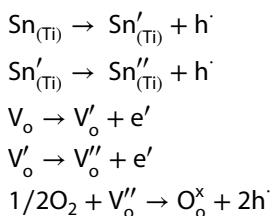

values less than unity. Figure 7 shows the increase in conductivity with increase in temperature. Electrical conductivity data fitted Arrhenius equation (Eq. 5)

$$\sigma = \sigma_0 \exp\left(-E_a/k_B T\right) \tag{5}$$

where σ_0 is the pre-exponential factor, E_a is the activation energy for conduction and k_B is Boltzmann constant. From Arrhenius plot (Fig. 8) energy of activation for conduction was calculated for both undoped and doped BaTiO$_3$ and found to be 0.65 and 0.63 eV respectively.

Activation energy in the ranges of 0.3–0.5 and 0.6–1.2 eV have been reported to be associated with singly and doubly ionized oxygen vacancies, respectively. Figure 8 shows the Arrhenius curve of conductivity with inverse of temperature. The calculated value of activation energy in the current system might be due to doubly ionized oxygen vacancies. The singly and doubly ionized oxygen vacancies can be calculated according to the following mechanism [19].

$$Sn_{(Ti)} \rightarrow Sn'_{(Ti)} + h^{\cdot}$$
$$Sn'_{(Ti)} \rightarrow Sn''_{(Ti)} + h^{\cdot}$$
$$V_o \rightarrow V'_o + e'$$
$$V'_o \rightarrow V''_o + e'$$
$$1/2 O_2 + V''_o \rightarrow O^x_o + 2h^{\cdot}$$

where $Sn_{(Ti)}$ represent neutral vacancies, $Sn'_{(Ti)}$ and $Sn''_{(Ti)}$ represent single and doubly ionized vacancies, respectively, $h^{\cdot}$ is the free electron hole, and V'_O and V''_O are the single and doubly ionized oxygen vacancies, respectively.

4 Conclusion

Sol gel method was used to synthesize nanosize BaTiO$_3$ and Sn^{2+} doped BaTiO$_3$ at 1200 °C. XRD studies showed the formation of solid solution and EDX confirmed the presence of tin in the lattice. XRD pattern showed cubic structure for doped BaTiO$_3$ as the peaks corresponding to (002) and (210) planes disappeared after doping. The dielectric constant of Sn^{2+} doped ceramic was found 3 times higher to that of pure BaTiO$_3$. The Sn^{2+} doped BaTiO$_3$ was found to be a ferroelectric material and can act as a promising material for piezoelectric applications because of high T$_c$ of around 290 °C.

Compliance with ethical standards

References

1. Selvaraj M, Venkatesan R, Mayandi J, Venkatachalapathy V (2019) Influence of tin (IV) doping on structural and optical properties of rhombohedral barium titanate (BaTiO$_3$). Mater Today Proc
2. Yu Z, Guo R, Bhalla AS (2000) Dielectric behavior of Ba(Ti$_{1-x}$Zr$_x$)O$_3$ single crystals. J Appl Phys 88:410–415
3. ChandramaniSingh K, Nath AK, Laishram R, Thakur OP (2011) Structural, electrical and piezoelectric properties of nanocrystalline tin-substituted barium titanate ceramics. J Alloy Compd 509:2597–2601
4. Liu W, Wang J, Ke X, Li S (2017) Large piezoelectric performance of Sn doped BaTiO$_3$ ceramics deviating from quadruple point. J Alloys Compd 712:1–6

5. Chihaoui S, Seveyrat L, Perrin V, Kallel I, Lebrun L, Khemakhem H (2017) Structural evolution and electrical characteristics of Sn-doped $Ba_{0.8}Sr_{0.2}TiO_3$ ceramics. Ceram Int 43:427–432

6. Wang J, Jiang S, Jiang D, Wang T, Yao H (2013) Effects of Sn on the microstructure and dielectric properties in $BaTiO_3$-based ceramics. Ceram Int 39:3657–3662

7. Suzuki S, Takeda T, Ando A, Oyama T, Wada N, Niimi H, Takagi H (2010) Effect of Sn^{2+} ion substitution on dielectric properties of (Ba, Ca)TiO_3 ferroelectric ceramics. Jpn J Appl Phys 49:904

8. Yi-Hsuan L, Lin W-H, Yang C-Y, Chiu Y-H, Ying-Chih P, Lee M-H, Tseng Y-C, Hsu Y-J (2014) A facile green antisolvent approach to Cu^{2+}- doped ZnO nanocrystals with visible-light-responsive Photoactivities. Nanoscale 6:8796–8803

9. Ying-Chih P, Chen Y-C, Hsu Y-J (2010) Au-decorated $Na_xH_{2-x}Ti_3O_7$ nanobelts exhibiting remarkable photocatalytic properties under visible-light illumination. Appl Catal B 97:389–397

10. Chen C-C, Hsu Y-J, Lin Y-F, Shih-Yuan L (2008) Superparamagnetism found in diluted magnetic semiconductor nanowires: Mn-Doped CdSe. J Phys Chem C 112:17964–17968

11. Hsieh P-L, Naresh G, Huang Y-S, Tsao C-W, Hsu Y-J, Chen L-J, Huang MH (2019) Shape-tunable $SrTiO_3$ crystals revealing facet-dependent optical and photocatalytic properties. J Phys Chem C 123:13664–13671

12. Hsu Y-J, Lu S-Y (2008) Dopant-induced formation of branched CdS nanocrystals. Small 4(7):951–955

13. Ganguly M, Rout SK, Sinha TP, Sharma SK, Park HY, Ahn CW, Kim IW (2013) Characterization and rietveld refinement of A-site deficient lanthanum doped barium titanate. J Alloys Compd 579:473–484

14. Royer S, Duprez D, Can F, Courtois X, Dupeyrat CB, Laassiri S, Alamdari H (2014) Perovskites as substitute of noble metals for heterogeneous catalysis: dream or reality. Chem Rev 114:10292–10368

15. Omari LH, Moubah R, Haddad M (2017) Conductivity and electrical impedance of $(BaTiO_3)_{0.95}$–$(LaFeO_3)_{0.05}$ Solid Solutions. Mater Chem Phys 199:138–143

16. Frattini A, Loreto AD, Sanctis OD (2013) Parameter optimization in the synthesis of BZT ceramics to achieve good dielectric properties. J Mater 393017:1–6

17. Maiti T, Guo R, Bhalla AS (2008) Structure-property phase diagram of $BaZr_xTi_{1-x}O_3$ system. J Am Ceram Soc 91(6):1769–1780

18. Sakayori K, Matsui Y, Abe H, Nakamura E, Kenmoku M, Hara T, Ishikawa D, Kokubu A, Hirota K, Ikeda T (1995) Curie temperature of $BaTiO_3$. Jpn J Appl Phys 34(9S):5443–5445

19. Gupta P, Kumar M, Nagarajan R (2018) Interplay between defects and cation nonstoichiometry in lithium substituted $CdGa_2O_4$ leading to multifunctional behavior. J Phys Chem C 122:22094–22105

20. Vijatovic Petrovic MM, Bobic JD, Banys J, Stojanovic BD (2013) Electrical properties of antimony doped barium titanate ceramics. Mater Res Bull 48:3766–3772

21. Takahashi H, Numamoto Y, Tani J, Tsurekawa S (2006) Piezoelectric properties of $BaTiO_3$ ceramics with high performance fabricated by microwave sintering. Jpn J Appl Phys 45(9B):7405–7408